Effect of Ca(II) on U(VI) and Np(VI) retention on Ca-bentonite and clay minerals at hyperalkaline conditions – New insights from batch sorption experiments and luminescence spectroscopy

Philipp, T.; Huittinen, N. M.; Shams Aldin Azzam, S.; Stohr, R.; Stietz, J.; Reich, T.; Schmeide, K.;

Originally published:

June 2022

Science of the Total Environment 842(2022), 156837

DOI: https://doi.org/10.1016/j.scitotenv.2022.156837

Effect of Ca(II) on U(VI) and Np(VI) retention on Ca-bentonite and clay minerals at hyperalkaline conditions – New insights from batch sorption experiments and luminescence spectroscopy

Thimo Philipp [a,1], Nina Huittinen [a], Salim Shams Aldin Azzam [a], Robin Stohr [b], Janina Stietz [b], Tobias Reich [b], Katja Schmeide [a,*]

[a] Helmholtz-Zentrum Dresden – Rossendorf e.V., Institute of Resource Ecology, Bautzner Landstraße 400, 01328 Dresden, Germany

[b] Johannes Gutenberg-Universität Mainz, Department of Chemistry, Fritz Strassmann Weg 2, 55128 Mainz, Germany

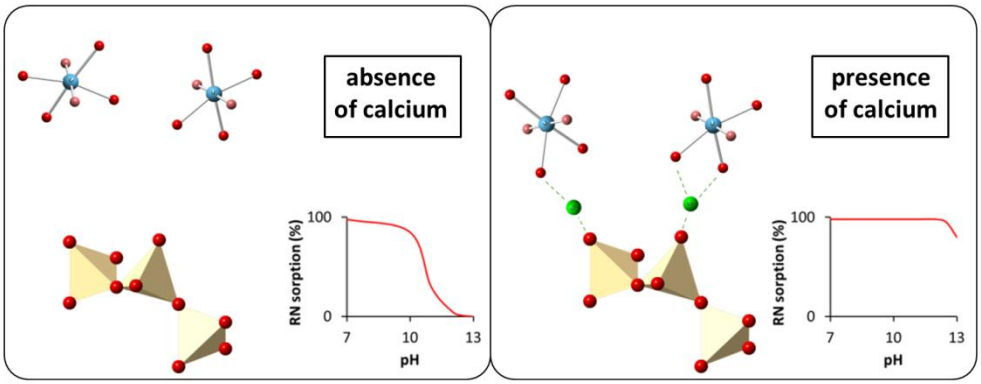

* Corresponding author: Dr. Katja Schmeide (E-mail address: k.schmeide@hzdr.de, phone: +49 351 260 2436).

[1] Present address: Federal Office for the Safety of Nuclear Waste Management (BASE), Wegelystraße 8, 10623 Berlin, Germany

Abstract

In deep geological repositories for radioactive waste, interactions of radionuclides with mineral surfaces occur under complex geochemical conditions involving complex solution compositions and high pH resulting from degradation of cementitious geo-engineered barriers. Ca^{2+} cations have been hypothesized to play an important role as mediators for the retention of U(VI) on Ca-bentonite at (hyper)alkaline conditions, despite the anionic character of both the mineral surface and the aqueous uranyl species. To gain deeper insight into this sorption process, the effect of Ca^{2+} on U(VI) and Np(VI) retention on alumosilicate minerals has been comprehensively evaluated, using batch sorption experiments and time-resolved laser-induced luminescence spectroscopy (TRLFS). Sorption experiments with Ca^{2+} or Sr^{2+} and zeta potential measurements showed that the alkaline earth metals sorb strongly onto Ca-bentonite at pH 8–13, leading to a partial compensation of the negative surface charge, thereby generating potential sorption sites for anionic actinyl species. U(VI) and Np(VI) sorption experiments in the absence and presence of Ca^{2+} or Sr^{2+} confirmed that these cations strongly enhance radionuclide retention on kaolinite and muscovite at $pH \geq 10$. Concerning the underlying retention mechanisms, site-selective TRLFS provided spectroscopic proof for two dominating U(VI) species at the alumosilicate surfaces: (i) A ternary U(VI) complex, where U(VI) is bound to the surface via bridging Ca cations with the configuration $surface \equiv Ca - OH - U(VI)$ and, (ii) U(VI) sorption into the interlayer space of calcium (aluminum) silicate hydrates (C-(A-)S-H), which form as secondary phases in the presence of Ca due to partial dissolution of alumosilicates under hyperalkaline conditions. Consequently, the present study confirms that alkaline earth elements, which are ubiquitous in geologic systems, enable strong retention of hexavalent actinides on clay minerals under hyperalkaline repository conditions.

Keywords: Kaolinite, Muscovite, Uranium, Calcium bridge, C-S-H, TRLFS

1. Introduction

The strategy followed by many countries to ensure the long-term containment of spent nuclear fuel and high-level radioactive waste is the final disposal in deep geological formations involving multiple protective barriers. Therefore, it is necessary to generate a profound understanding of the interactions between radionuclides (RNs) and mineral surfaces under the conditions expected in a deep geological waste repository.

The chemical system in the near-field of a nuclear waste repository is very complex. It is influenced by the presence of different materials as components of a multi-barrier system, consisting of three principal parts: technical barriers (steel or copper containers enclosing the nuclear waste), geotechnical barriers (e.g., bentonite, cementitious materials, asphalt/bitumen elements), and the geological barrier (argillaceous, crystalline or salt host rock) (OECD/NEA, 2020). In most repository concepts, bentonite, a natural swelling clay with high montmorillonite content, will be used as buffer and backfill material (Jenni et al., 2019; Kaufhold and Dohrmann, 2016; Lommerzheim and Jobmann, 2014). Due to its good sealing properties and high sorption capacity for radiotoxic and/or chemotoxic waste components, the bentonite is expected to protect and isolate the canisters containing the waste and to retain and retard RNs in case of canister degradation and failure. Cementitious materials, used for concrete lining and concrete plugs in the repository, are applied to ensure mechanical stability and sealing of disposal tunnels and galleries.

Natural pore waters in deep geological formations feature a complex composition, containing several cations and anions which could either form stable complexes with potentially released RNs or compete with the RNs for sorption sites on available mineral surfaces. These pore waters can have considerably high ionic strengths. For instance, in North German clay formations, which are considered as potential host rocks, salinities of about 150 g/L are expected in the lower cretaceous claystones at 800 m depth (Nowak and Maßmann, 2013; Wolfgramm et al., 2011). High salinities promote the corrosion of concrete within the geotechnical barrier, leading to the evolution of hyperalkaline cement pore waters ($10 < pH < 13$) (Berner, 1992; Gaucher et al., 2006) with enhanced Ca^{2+} contents. The strongly increased alkalinity of contact waters in turn can lead to mineral alterations of the bentonite backfill and formation of secondary phases and, moreover, can modify RN

speciation. Altogether, these processes can affect the RN retention potential of bentonite. Hence, laboratory studies on RN sorption on mineral surfaces must preferably be conducted in consideration of multi-mineral solid phases, complex solution composition, high ionic strength, high pH values and low RN concentrations.

Most RN retention/diffusion studies with argillaceous rocks or clay minerals have been conducted either at a pH representative of natural clay pore water or in the pH range of approximately 3 to a maximum of 10, and predominately at low ionic strengths (Hennig et al., 2020; Joseph et al., 2017; Joseph et al., 2013b; Marques Fernandes et al., 2012; Schmeide and Bernhard, 2010; Tran et al., 2018; Wu et al., 2009). Only few RN retention studies were performed at increased ionic strengths (Marsac et al., 2017; Nagasaki et al., 2016; Schnurr et al., 2015; Scholze et al., 2019; Stockmann et al., 2022). Even less RN retention studies were performed at increased ionic strengths and hyperalkaline conditions. In our recent study, U(VI) retention on Ca-bentonite was investigated in the pH range 8–13 and at increased ionic strength applying the so called 'diluted Gipshut solution' (2.5 M NaCl, 0.02 M $CaCl_2$, 0.02 M Na_2SO_4, and 0.0051 M KCl; I = 2.63 M) as background electrolyte (Philipp et al., 2019). Despite the fact that both the bentonite surface and the prevailing aqueous uranyl complexes are negatively charged in this high pH range, the results showed a strong U(VI) retention onto Ca-bentonite up to pH 12. Uranyl carbonates do not play a role at hyperalkaline conditions due to the predominance of uranyl hydrolysis. The retention of U(VI) reached its maximum at conditions where $UO_2(OH)_3^-$ dominated the aqueous speciation. By means of site-selective TRLFS (at 10 K) and X-ray absorption fine structure (EXAFS) spectroscopy, two independent U(VI) sorption species were detected on Ca-bentonite at pH 8–13, whereas U(VI) precipitation was excluded. With increasing pH, the nature of the retained U(VI) complexes shifted from bidentate inner-sphere surface complexes with an overall equatorial coordination of five, adsorbed on aluminol or silanol edge sites, to a surface complex with a 4-fold equatorial coordination, resembling the aqueous species $UO_2(OH)_4^{2-}$. Concerning the character of this latter sorption species at very high pH, it was hypothesized that the binding of the anionic uranyl hydroxide complexes to the negatively charged surface is mediated by Ca^{2+} cations (Philipp et al., 2019). This hypothesis was recently supported by Brix et al. (2021), who observed higher U(VI) retention in hyperalkaline chemical systems with higher Ca^{2+} concentrations

and proposed a bridging effect of Ca^{2+}. Using calcium silicate hydrate (C-S-H) phases, which are major constituents of fresh and degraded cement, as an example, Androniuk and Kalinichev (2020) proposed complex formation between $UO_2(OH)_3^-$ and Ca^{2+} sorbed on negatively charged silanol groups based on molecular dynamics simulations. However, spectroscopic proof of the existence of such complexes under hyperalkaline conditions is still missing.

Therefore, the focus of the present paper is the detailed study of the potential effect of Ca^{2+} on U(VI) retention onto clay mineral surfaces at hyperalkaline conditions, and the unambiguous description of the underlying sorption mechanisms. Consequently, the sorption of Ca^{2+} on the naturally occurring clay rock Ca-bentonite and its effect on the bentonite surface charge was studied at pH 8–13. In addition, to quantify the influence of Ca^{2+} on U(VI) sorption on Ca-free mineral phases, U(VI) batch sorption experiments were conducted with the clay mineral kaolinite as well as with the clay mineral analogue muscovite in 0.1 M NaCl as well as in 0.1 M NaCl + 0.02 M $CaCl_2$ at pH 8–13. Furthermore, equivalent batch sorption experiments were performed in the presence of Sr^{2+} instead of Ca^{2+} and with Np(VI) in order to elucidate whether the observed phenomena are similarly valid for other alkaline earth metals as well as other hexavalent actinides. To address the underlying retention mechanisms occurring at these clay mineral surfaces, laser-induced luminescence spectroscopy was applied to identify U(VI) sorption species in the absence and presence of Ca^{2+}.

2. Materials and methods

2.1. Materials

The Ca-bentonite was of the type Calcigel® (Clariant, Munich, Germany) with a mineral composition of 60–70% montmorillonite, 6–9% quartz, 1–6% mica, 1–4% feldspar, 1–2% kaolinite and 5–10% others (supplier information). Particle sizes range between 0.5 and 150 µm with the dominant fraction (90%) of the particles being smaller than 90 µm; the BET specific surface area (SSA) was determined to be 76.5 m^2/g (Philipp et al., 2019).

Synthetic kaolinite was obtained as described in Huittinen et al. (2010) by hydrothermal treatment of an aluminosilica gel at 220 °C according to the procedure by Fialips et al. (2000). The SSA was

determined to be 22.2 m^2/g. The particle size was < 1.1 µm as observed by SEM; EDX mapping revealed that the synthetic kaolinite did not contain any impurities (the only elements detected were O, Al and Si) (Huittinen et al., 2010). Natural kaolinite from Georgia (KGa-1b) was obtained from the Source Clay Repository of the Clay Minerals Society, it was used as received. The SSA was determined to be 11.7 m^2/g. Its chemical and mineralogical characterization is given in Pruett and Webb (1993).

Muscovite single crystals (12.7 × 12.7 × 0.2 mm^3) were purchased from the Asheville-Schoonmaker Mica Company (USA) and milled to a fine powder with an agate ball mill. The grain size fraction < 63 µm of the mineral powder was used for the batch sorption experiments. Its SSA was determined to be 9.9 m^2/g (Hellebrandt, 2017).

The elemental composition of these minerals is shown in Table S1 (Supplementary Material).

For comparison purposes, a U(VI)-doped calcium silicate hydrate (C-S-H) phase with a Ca/Si ratio of 1.2 was synthesized in alkali-free solution according to the procedure described in Wolter et al. (2019b). The equilibration time was 67 d, the final U(VI) loading was 8.3×10^{-4} mol/kg at a pH of 12.1.

Background electrolytes in the sorption experiments were either pure NaCl (p.a., Carl Roth, Karlsruhe, Germany) solutions as well as mixed NaCl/$CaCl_2$ (puriss. AppliChem, Darmstadt, Germany) or NaCl/$SrCl_2$ (p.a., Merck, Darmstadt, Germany) solutions. All solutions were prepared with deionized water (18.2 MΩ cm; mod. Milli-RO/Milli-Q-System, Millipore, Schwalbach, Germany) which was additionally degassed prior to solution preparation by boiling for about 2 h to avoid any introduction of CO_2 and O_2 and was purged for several minutes with Ar in case of Np(VI) sorption experiments.

Added U(VI) originated from a 1×10^{-3} M stock solution (U_{nat} in 0.005 M $HClO_4$). The ^{237}Np(VI) stock solution, where ^{237}Np was in secular equilibrium with ^{233}Pa, was prepared as described in Amayri et al. (2011). The ^{45}Ca stock solution was purchased from PerkinElmer (Waltham, USA) as $^{45}CaCl_2$ in aqueous solution and had a tracer concentration of 2×10^{-11} M.

2.2. Batch sorption experiments

Experiments were performed in glove boxes under carbonate-free, inert gas atmosphere: N_2 (U(VI) experiments) or Ar (Np(VI) experiments). The mineral powders were weighed in 15 mL polypropylene centrifuge tubes (Greiner Bio-One, Frickenhausen, Germany) and suspended with 10 mL of the respective background electrolyte. The experimental parameters of all batch sorption experiments are compiled in Table 1. All sorption samples were prepared in duplicate.

In the experiments with U(VI), suspensions were pre-conditioned with pH-adjustments by diluted NaOH (p.a., Carl Roth) or HCl (p.a., ACS, ISO, Carl Roth) every other day until a constant pH value (±0.05) was reached (approx. two weeks). The pH was measured with an InoLab pH 7110 pH meter (WTW, Weilheim, Germany) and a SenTix MIC glass electrode (WTW). Three point calibration was executed with WTW buffer solutions (pH 6.865, 9.180 and 12.454; WTW). During pre-equilibration, samples were placed in an end-over-end rotator.

In the experiments with Np(VI), pH and E_h values were measured with an inoLab pH/Cond 720 meter (WTW), equipped with a temperature sensor WTW TFK 150. The BlueLine 16 pH electrode (Schott Instruments GmbH, Mainz, Germany) was calibrated using certified DIN buffer solutions (see above). The BlueLine 31 Rx redox electrode (Schott Instruments) was checked regularly with a +640 mV redox standard (Schott Instruments). The redox potentials measured against Ag/AgCl were converted to standard hydrogen electrode (SHE) by adding 210 mV to the measured potential.

After pre-equilibration, U(VI), Np(VI) or Ca^{2+} were added to the suspensions by pipetting calculated volumes of the respective stock solution. In the experiments with Np(VI), its hexavalent oxidation state was prepared by fuming a ^{237}Np stock solution several times with 1 M $HClO_4$, but never to complete dryness. The oxidation state +VI was stabilized by addition of an aliquot of 2 M NaClO to the kaolinite suspensions to yield a hypochlorite concentration of 0.02 M in the batch samples. The concentration and the oxidation state of ^{237}Np in the stock solution were determined by γ-ray spectroscopy and UV-Vis spectroscopy, respectively. In the Ca sorption experiments, $CaCl_2$ spiked with 1×10^{-12} M $^{45}Ca^{2+}$ was used for the stock solution. Initial RN concentrations in the different experiments are listed in Table 1.

Table 1: Experimental parameters of the batch sorption experiments.

RN	Experiment	Mineral	Electrolyte	S/L / g/L	[RN] / M	pH
U(VI)	pH edge	Ca-bentonite	0.1 M NaCl	10	5×10^{-7}	8-13
		syn. kaolinite	0.1 M NaCl	0.5	5×10^{-7}	10-13
			0.1 M NaCl + 0.02 M $CaCl_2$	0.5	5×10^{-7}	10-13
		muscovite	0.1 M NaCl	3	5×10^{-7}	8-13
			0.1 M NaCl + 0.02 M $CaCl_2$	3	5×10^{-7}	8-13
			0.1 M NaCl + 0.02 M $SrCl_2$	3	5×10^{-7}	10-13
Np(VI)	pH edge	nat. kaolinite	0.1 M NaCl	3	1×10^{-7}	8-12
			0.1 M NaCl + 0.02 M $CaCl_2$	3	1×10^{-7}	8-12
Ca(II)	S/L ratio	Ca-bentonite	-	0.2-20	2×10^{-4}	10
	pH edge	Ca-bentonite	-	10	2×10^{-4}	8-13

The sorption time was always seven days for U(VI) and three days for Np(VI) based on previous kinetic sorption experiments (Amayri et al., 2011; Philipp et al., 2019). Sorption time for Ca^{2+} was one day. During this time, the samples were rotated in an end-over-end shaker. Final pH values were determined at the end of the sorption experiments.

For phase separation, U(VI) and Ca^{2+} sorption samples were centrifuged at 6800×g for 30 min in an Avanti J-20 XP centrifuge (Beckman Coulter, Fullerton, USA). Np(VI) samples were separated at 4025×g for 60 min in a SIGMA 3K30 centrifuge (Sigma Laborzentrifugen GmbH, Osterode, Germany).

U_{nat} and Ca concentrations in the supernatants were measured by ICP-MS (NexION 350X, PerkinElmer, Waltham, USA), while equilibrium concentrations of ^{237}Np after sorption were determined by ICP-MS (Agilent ICP-MS 7500ce, Agilent Technologies, Santa Clara, CA, USA). ^{45}Ca concentrations in the supernatants were determined by liquid scintillation counting (LSC; Winspectral α/β, Wallac 1414, PerkinElmer, USA), using an Ultima Gold™ scintillation cocktail (PerkinElmer).

From the initial (c_0) and equilibrium (c_{eq}) RN concentrations in solution (M), the percentage of RN sorption was calculated according to Eq. (1).

$$RN\ sorbed\ /\ \% = \frac{c_0 - c_{eq}}{c_0} \times 100\% \quad (1)$$

2.3. Zeta potential measurements

The surface charge of Ca-bentonite particles was determined by zeta potential measurements (Zetasizer Nano ZS, Malvern Instruments, Malvern, United Kingdom). A total of eleven Ca-bentonite suspensions (0.1 g/L) in the pH range 8–13 were prepared in each 0.1 M NaCl, 0.1 M NaCl + 0.02 M $CaCl_2$ and 0.1 M NaCl + 0.02 M $SrCl_2$ in order to evaluate the effect of pH, ionic strength and Ca^{2+} or Sr^{2+} concentrations on the surface charge. Results were averaged over ten measurements, each consisting of 10–50 scans.

2.4. Luminescence spectroscopy

Site-selective TRLFS was applied to investigate the U(VI) species sorbed on the surface of Ca-bentonite, muscovite and kaolinite. Samples were prepared under carbonate-free N_2 atmosphere as described in section 2.2 but with lower S/L ratio (0.3 g/L) in order to increase the U(VI) surface coverage. Two samples were prepared with Ca-bentonite in diluted Gipshut solution (2.5 M NaCl, 0.02 M $CaCl_2$, 0.02 M Na_2SO_4, and 0.0051 M KCl; I = 2.63 M) at pH 11, where sorption is at maximum: One with the same U(VI) concentration as in the pH-dependent sorption experiments (5×10^{-7} M) and one with a U(VI) concentration two orders of magnitude higher than that (5×10^{-5} M) to provoke U(VI) precipitation for comparison. Additionally, one sample was prepared with Ca-bentonite in diluted Gipshut solution at pH 12.5.

U(VI) sorption on muscovite was investigated in 0.1 M NaCl at pH 11 and in 0.1 M NaCl + 0.02 M $CaCl_2$ at pH 12. Kaolinite samples were prepared in 0.1 M NaCl at pH 10 and in 0.1 M NaCl + 0.02 M $CaCl_2$ at pH 12. To account for potential formation of C-S-H phases in the Ca-containing mineral suspensions and the subsequent association of U(VI) with this secondary phase, also the U(VI) speciation on a synthetic U(VI)-doped C-S-H phase was investigated (Ca/Si = 1.2, U(VI) loading = 8.3×10^{-4} mol/kg, pH 12.1).

Prior to the spectroscopic measurements, the samples were ultracentrifuged (187,000×g), and the wet paste pellets were transferred into copper sample holders with a sealable quartz glass lid. The

sorption samples were measured with a pulsed Nd:YAG (Continuum Surelite II, San Jose, USA) pumped dye laser setup (Radiant Dyes Narrow Scan K, Wermelskirchen, Germany). The C-S-H sample was measured with a tunable diode pumped solid state (DPSS) laser (Ekspla, NT230, Vilnius, Lithuania). The emitted luminescence light was directed into a spectrograph (Shamrock 303iAndor Oxford Instruments, Abingdon, United Kingdom) equipped with a polychromator with 300, 600, and 1200 lines/mm gratings, and the emission was monitored with an intensified CCD camera (Andor iStar, Oxford Instruments) 10 µs after the exciting laser pulse in a time window of 10 ms. The sorption samples were excited in the wavelength range between 460 and 520 nm with a step size of 0.2 nm. During these measurements, the laser pulse energy and the exact excitation wavelength were monitored with an optical power meter (Newport 1918-R, Irvine, USA) and a wavelength meter (High Finesse WS-5, Tübingen, Germany), respectively. U(VI) associated with the C-S-H phase was excited in the wavelength range between 340 and 390 nm due to a lower suppression of the laser signal using the DPSS laser set-up.

Additionally, time-resolved luminescence spectra were recorded at selected excitation wavelengths with a temporal step size of 10 µs. To achieve the desired spectral resolution, the solid samples were cooled to ~10 K in a helium-refrigerated cryostat.

3. Results and discussion

3.1. Ca(II) and Sr(II) sorption on Ca-bentonite at (hyper)alkaline conditions

The sorption of Ca^{2+} on Ca-bentonite was investigated in batch sorption experiments as a function of S/L ratio and pH value. The initial Ca^{2+} concentration of 2×10^{-4} M was chosen based on estimations for a monolayer saturation of the Ca-bentonite surface with Ca^{2+} cations considering the literature value for the montmorillonite surface site density of 2×10^{-5} mol/g (Wieland et al., 1994).

The batch experiments as a function of S/L ratio prove that Ca^{2+} strongly adsorbs to the Ca-bentonite surface, when enough solid is present (i.e., sufficient sorption sites are available) (Fig. 1a), reaching a plateau of > 90% sorption at S/L ratios above 2 g/L. Based on these results, a S/L ratio of 10 g/L was chosen for the pH-dependent sorption experiments, in order to provide enough sites for unrestricted Ca^{2+} adsorption. As shown in Fig. 1b, sorption of Ca^{2+} was very high in the whole

investigated pH range 8–13. Sorption increases with increasing pH from 88% at pH 8 to a maximum of 97% at pH 11. The slight decrease to 86% sorption at pH 13 is attributed to a beginning dissolution of minerals within the bentonite, as observed in leaching experiments in Philipp et al. (2019). Strong retention of Ca^{2+} and its chemical analogue Sr^{2+} has already been observed on bentonite (Cherian et al., 2018; He et al., 2016; Missana and García-Gutiérrez, 2007; Missana et al., 2008), montmorillonite (Sugiura et al., 2021), muscovite (Fenter et al., 2007; Schlegel et al., 2006), kaolinite (Chen et al., 2014), illite (Fuller et al., 2016), silica and alumina (Szymanek et al., 2021). At pH < 8, the predominant retention mechanism is cation exchange, which is largely independent of pH, but highly sensitive to ionic strength (Missana and García-Gutiérrez, 2007). At pH > 8, also surface complexation contributes to the retention of Ca^{2+}. Missana and García-Gutiérrez (2007), Sugiura et al. (2021) and Szymanek et al. (2021) were only able to model an observed increase in Ca^{2+} sorption at pH > 8 by the introduction of surface complexes on the amphoteric edge sites of the minerals.

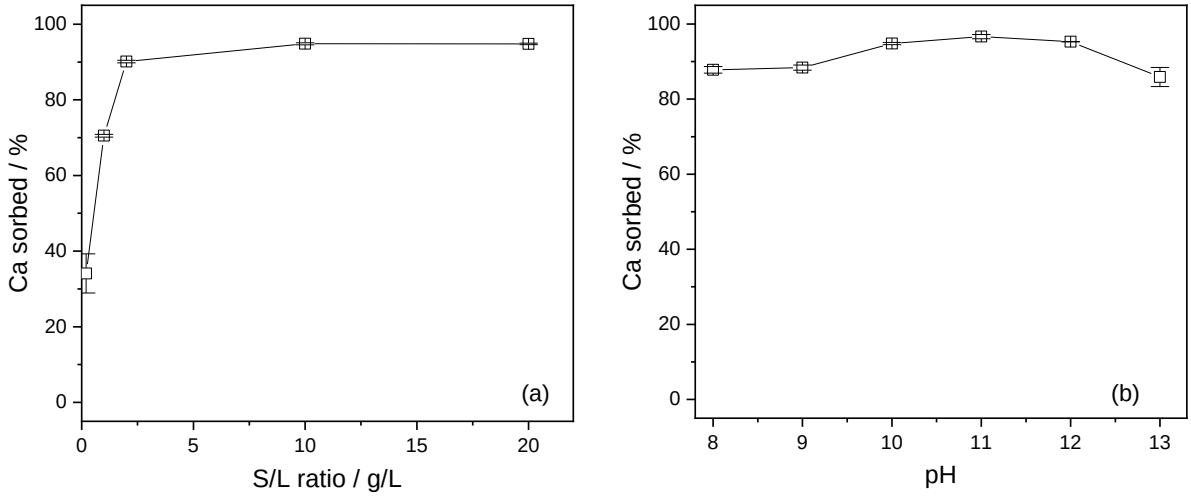

Figure 1: Sorption of calcium (2×10^{-4} M spiked with 1×10^{-12} M ^{45}Ca) on Ca-bentonite as a function of S/L ratio (pH 10) (a) and as a function of pH (S/L = 10 g/L) (b). The corresponding K_d-based graphs are shown in Fig. S1 (Supplementary Material).

An increase of the pH value leads to a successive deprotonation of the clay mineral surface ($SOH \leftrightarrow SO^- + H^+$), promoting surface complexation. Accordingly, Schlegel et al. (2006) and Fenter et al. (2007) also observed a contribution of surface complexation to Ca^{2+} and Sr^{2+} adsorption on the mica (001) surface, expressed in the partial removal of the hydration shell. Consequently, surface

complexation is assumed to contribute significantly to the strong Ca^{2+} retention on Ca-bentonite at pH 8–13 observed in the present study.

The adsorption of Ca^{2+} on the Ca-bentonite surface is additionally evidenced by the measurement of the zeta potential of Ca-bentonite with added $CaCl_2$. Compared to the measurement in pure 0.1 M NaCl, the addition of 0.02 M Ca^{2+} leads to a much less negative surface charge over the entire investigated pH range 7–13 (Fig. 2). Part of the difference can be explained by the exchange of Ca^{2+} by Na^+ in the Ca-bentonite upon suspension in NaCl, commonly evoking more negative surface charge. However, the fact that the zeta potential does not become more negative with increasing pH in the presence of Ca^{2+} and strongly increases at pH > 10 proofs additional surface complexation of Ca^{2+}. The presence of Ca^{2+} does not result in a complete reversal of surface charge, however, negative surface charge is partly compensated. As the average charge of all existing surface sites is measured with this bulk technique, a partial compensation of negative surface charge implies the existence of locally positively charged sites due to surface complexation of Ca^{2+}. Beside the effect of Ca^{2+}, also the influence of Sr^{2+} on the surface charge was investigated. In 0.1 M NaCl + 0.02 M $SrCl_2$, the effect on the surface charge is almost identical to the experiment with Ca^{2+} (Fig. 2). Both divalent cations, Ca^{2+} and Sr^{2+}, having the same charge compensating effect, indicate that the charge of the cation is the main driving factor for the observed changes in the zeta potential.

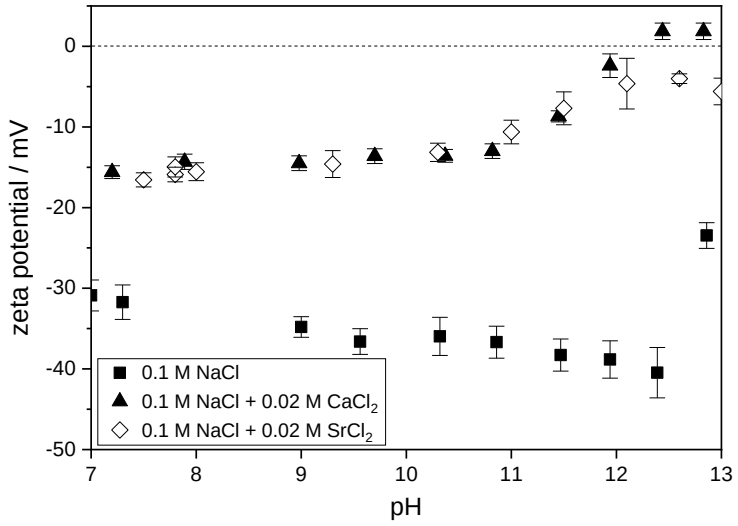

Figure 2: Surface potential of Ca-bentonite (0.1 g/L) as a function of pH value and background electrolyte.

Similar impact on surface charge due to adsorption of Ca^{2+} at alkaline conditions has been previously reported for different types of bentonite (Cherian et al., 2018; Ho and Handy, 1963), kaolinite (Atesok et al., 1988; Farooq et al., 2011), alumina and silica (Szymanek et al., 2021) and cementitious material (Pointeau et al., 2006; Viallis-Terrisse et al., 2001). In some of these studies even a reversal of charge was observed.

Both batch sorption experiments with Ca^{2+} and zeta potential measurements have shown that Ca^{2+} strongly adsorbs to the Ca-bentonite surface and consequently, generates alternative sorption sites for anionic actinyl hydroxides. The resulting Ca-induced changes in U(VI) and Np(VI) sorption are presented in section 3.2.

3.2. Effect of Ca(II) and Sr(II) on U(VI) and Np(VI) sorption on Ca-bentonite, kaolinite and muscovite

As the previous U(VI) sorption experiments on Ca-bentonite in diluted Gipshut solution were conducted in the presence of Ca^{2+} (Philipp et al., 2019), the aim was to perform similar experiments, but with the exclusion of Ca^{2+}. For that purpose, mineral suspensions were prepared in NaCl background solutions instead of the diluted Gipshut solution. Moreover, in addition to Ca-bentonite, the mineral phases kaolinite and muscovite, which do not contain intrinsic Ca that could be leached during the experiment but serve as analogues for montmorillonite/bentonite, were chosen for further batch sorption experiments. Assuming that Ca^{2+} is responsible for enabling sorption of actinyl hydroxide complexes, U(VI) and Np(VI) retention is expected to be radically decreased in these experiments between pH 10 and 12 compared to their retention in the presence of Ca^{2+}.

3.2.1. U(VI) sorption on Ca-bentonite

The batch sorption experiments in our previous study (Philipp et al., 2019) have shown a very high U(VI) retention on Ca-bentonite in diluted Gipshut solution up to pH 12. Only at pH > 12, sorption decreased to approx. 50% at pH 13. The concentrations of Ca^{2+} in these samples were very high due to the composition of the diluted Gipshut solution (2.5 M NaCl, 0.02 M $CaCl_2$, 0.02 M Na_2SO_4, and 0.0051 M KCl). In the present study, the experiment was repeated in only 0.1 M NaCl background electrolyte. The obtained results are very similar to the experiment with diluted Gipshut

solution (Fig. 3). Apart from a slight decline of the U(VI) uptake at a pH around 9, likely due to a minor intrinsic carbonate impurity in the Ca-bentonite material, a very high U(VI) retention up to pH 12 can be seen. Uranyl carbonate species have been shown to reduce U(VI) sorption in previous studies (Meleshyn et al., 2009; Stockmann et al., 2022), however, as the pH increases, the role of carbonates decreases as U(VI) hydroxo complexes become prevailing. The decrease in sorption above pH 12 is slightly more pronounced in the experiment with 0.1 M NaCl (Fig. 3). However, the postulated drop of U(VI) retention at pH > 10 due to the absence of Ca could not be observed. In fact, still considerably high Ca concentrations, leached from Ca-bentonite, were detected in the supernatants (e.g., 9.8×10^{-4} M at pH 11). Previous leaching tests with the Ca-bentonite revealed that Ca is released from the mineral phase into the solution under the given conditions (Philipp et al., 2019). That means that Ca-free sorption samples with a potentially different U(VI) sorption behavior can only be obtained with other mineral phases which do not contain any Ca that could potentially be leached.

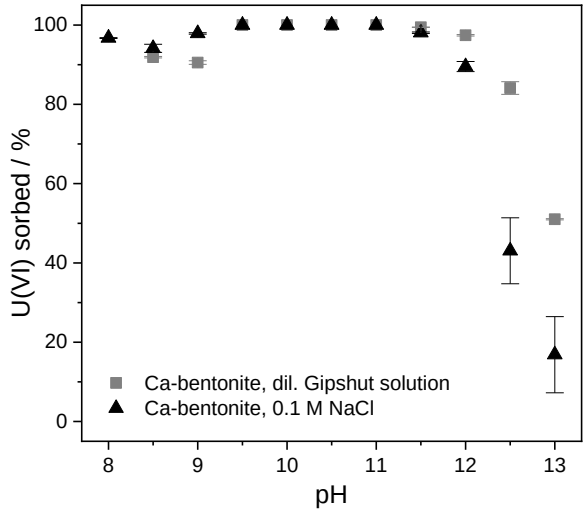

Figure 3: U(VI) sorption ([U(VI)] = 5×10^{-7} M) on Ca-bentonite (10 g/L) in 0.1 M NaCl as a function of pH. The U(VI) sorption on Ca-bentonite ([U(VI)] = 5×10^{-7} M, 10 g/L) in diluted Gipshut solution is shown for comparison (Philipp et al., 2019). The corresponding K_d-based graphs are shown in Fig. S2.

3.2.2. U(VI) sorption on synthetic kaolinite

Experiments were performed at pH 10, 11, 12 and 12.7 both in 0.1 M NaCl and 0.1 M NaCl + 0.02 M $CaCl_2$ (Fig. 4a). In contrast to the experiments with Ca-bentonite, the sorption of U(VI) on synthetic kaolinite is decreasing dramatically at pH ≥ 10 in the absence of Ca^{2+}. At pH 12, sorption

reaches 0%, supporting the hypothesis that high U(VI) retention at pH 10–12 cannot be sustained in the absence of Ca^{2+}. Measured Ca^{2+} concentrations in the supernatant after the sorption experiment were as low as 4×10^{-6} M. This seems to be sufficiently low to prevent U(VI) sorption to the mineral surface at hyperalkaline conditions. The origin of trace amounts of Ca^{2+} in the supernatant could be contamination of laboratory equipment such as the pH electrode, or impurity of the NaCl electrolyte.

Experiments with added $CaCl_2$ were performed in order to verify that the decreased U(VI) retention at pH ≥ 10 is really associated to the lower Ca^{2+} concentration and not to the different mineral structure of kaolinite compared to Ca-bentonite. In 0.1 M NaCl + 0.02 M $CaCl_2$, U(VI) sorption on kaolinite is very high (> 80%) up to pH 12.7 (Fig. 4a). Therefore, it can be unequivocally concluded that the presence of Ca significantly enhances U(VI) retention between pH 10 and 13.

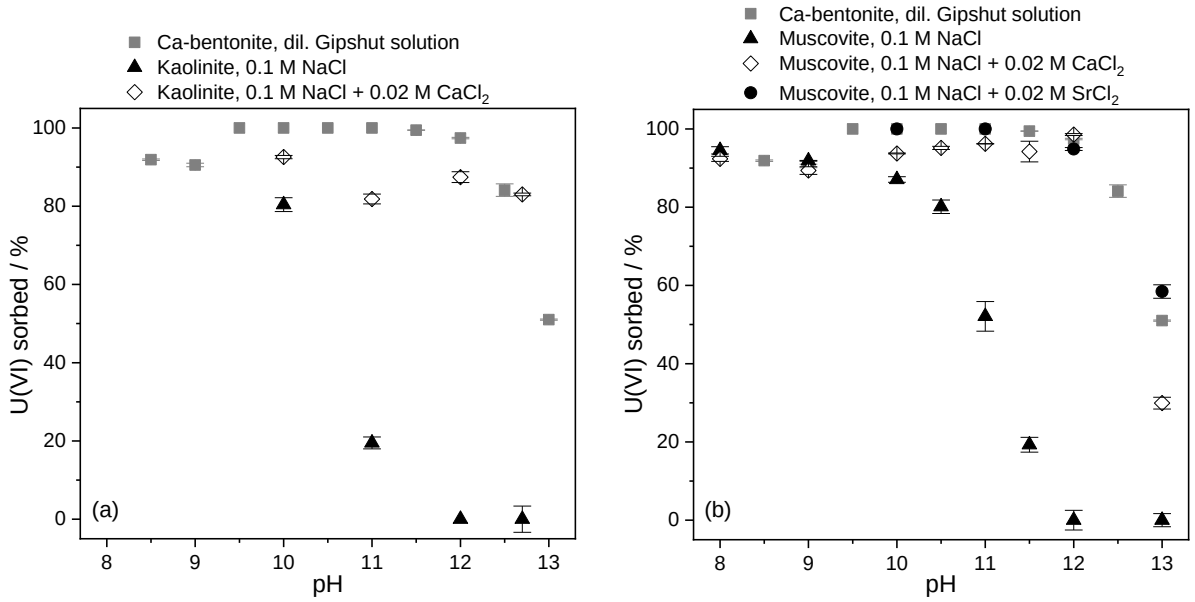

Figure 4: U(VI) sorption ([U(VI)] = 5×10^{-7} M) on synthetic kaolinite (0.5 g/L) (a) and muscovite (3 g/L) (b) in 0.1 M NaCl, 0.1 M NaCl + 0.02 M $CaCl_2$ and 0.1 M NaCl + 0.02 M $SrCl_2$ as a function of pH. The U(VI) sorption on Ca-bentonite ([U(VI)] = 5×10^{-7} M, 10 g/L) in diluted Gipshut solution is shown for comparison (Philipp et al., 2019).

3.2.3. U(VI) sorption on muscovite

The U(VI) sorption on muscovite is comparable to that of kaolinite (Fig. 4b). In 0.1 M NaCl, U(VI) sorption decreases first slowly at pH > 8 and then rapidly at pH ≥ 10, reaching 0% at pH 12. Measured Ca^{2+} concentrations in the supernatant after the sorption experiment were about 6.3×10^{-6} M, apparently low enough to not trigger substantial U(VI) retention.

The experiments with addition of $CaCl_2$ exhibit a high U(VI) sorption up to pH 12 and follow a similar trend as sorption experiments with Ca-bentonite (Fig. 4b). Thus, as already concluded for synthetic kaolinite, the low retention at pH ≥ 10 in 0.1 M NaCl is not a consequence of the different mineral structure but is directly related to the absence of Ca^{2+}.

A complementary pH-dependent U(VI) sorption experiment was conducted in 0.1 M NaCl + 0.02 M $SrCl_2$ in order to investigate if the presence of Sr^{2+} can have the same positive effect on U(VI) retention as Ca. As shown in Fig. 4b, in the presence of Sr^{2+} indeed an almost identical U(VI) sorption behavior was observed, with very high U(VI) retention up to pH 12. This suggests that the effect of enabling U(VI) adsorption is not attributed to exclusive properties of Ca^{2+} but to the charge of bivalent cations in general. The underlying retention mechanisms are further discussed in section 3.4.

3.2.4. Np(VI) sorption on kaolinite KGa-1b

The sorption of Np(VI) on natural kaolinite (KGa-1b) was studied in the pH range 8–12 using two different electrolytes, i.e., 0.1 M NaCl without and with addition of 0.02 M $CaCl_2$ (Fig. 5). To ensure the stability of the +VI oxidation state of Np, strongly oxidizing conditions were provided by the addition of 0.02 M NaClO. As can be seen from the Pourbaix diagram (Fig. S3), the measured E_h values indicate the dominance of Np(VI) in the pH range studied.

The sorption of Np(VI) on kaolinite in the pH range 8.0–10.5 is between 89–97% and independent of the presence of Ca^{2+} (Fig. 5). Above pH 11.0, Np(VI) sorption decreases strongly in the absence of Ca^{2+}, from 79% to 17% at pH 12. In the experiments with 0.02 M $CaCl_2$ in the background electrolyte, sorption remains above 80% in the pH range 11.0–11.5, reaching 90% at pH 12. The shallow minimum in the sorption curve between pH 11 and 12 in the presence of Ca^{2+} can be explained by two competing effects, i.e., decreasing sorption in 0.1 M NaCl and increasing Np(VI) retention under the influence of Ca^{2+}. A similar shallow minimum can be seen in the sorption data of U(VI) on synthetic kaolinite (Fig. 4a).

The precipitation of Ca neptunates in this pH range can be excluded under the experimental conditions. Fellhauer et al. (2018) studied the solubility of Ca_xNpO_{3-x}(hyd,s) in alkaline $CaCl_2$ solutions. For example, the Np(VI) equilibrium concentration in 0.25 M $CaCl_2$ in the pH range 8.8–

12.0 was equal to approximately 5×10^{-7} M Np(VI) (see Fig. 6a in Fellhauer et al. (2018)). The equilibrium concentration in the present batch experiment with 0.1 M NaCl + 0.02 M $CaCl_2$ at pH 12.0 was about one order of magnitude lower, i.e., approximately 1×10^{-8} M Np(VI).

The decrease of Np(VI) sorption at pH > 10 in the Ca-free background electrolyte is not as pronounced as observed for the U(VI) sorption on synthetic kaolinite (Fig. 4a). This can be explained by the fact that, in contrast to the synthetic kaolinite, the natural kaolinite contains small amounts of Ca (see Table S1) that can be leached during the sorption experiment.

Nonetheless, the sorption experiments with Np(VI) confirm the strong influence of Ca^{2+} on the retention of hexavalent actinides on kaolinite in the hyperalkaline pH range. Due to the similar chemistry and aqueous speciation of Np(VI) and U(VI) (Fig. S4), underlying retention mechanisms are expected to be equivalent. These are elucidated with the help of U(VI) luminescence spectroscopy in the following section.

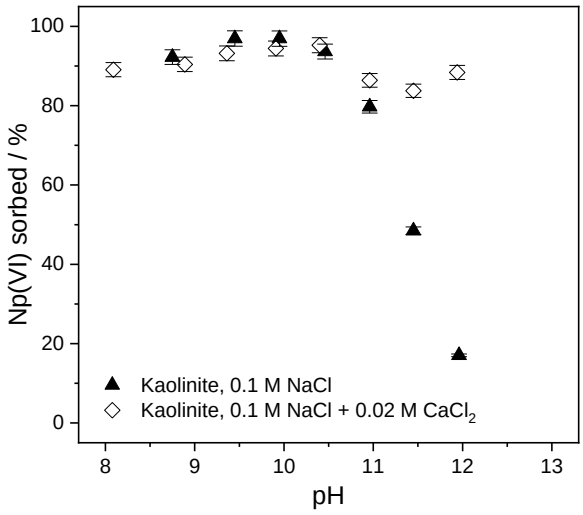

Figure 5: Np(VI) sorption ([Np(VI)] = 1×10^{-7} M) on kaolinite KGa-1b (3 g/L) in 0.1 M NaCl and 0.1 M NaCl + 0.02 M $CaCl_2$ as a function of pH under oxidizing conditions (0.02 M NaClO) and Ar atmosphere.

3.3. Site-selective TRLFS of Ca-induced U(VI) surface complexes

The site-selective TRLFS investigations of U(VI) sorption on the various alumosilicate minerals were conducted in two pH regimes: at pH 10 (kaolinite) or 11 (Ca-bentonite, muscovite), where the effect of Ca^{2+} on U(VI) sorption on the solid phases is small or negligible, and at pH 12–12.5, where Ca^{2+} has a strong effect on U(VI) retention. In case of muscovite and kaolinite, the sorption

experiments were performed in the absence (pH 10–11) and presence of 0.02 M Ca (pH 12–12.5), whereas diluted Gipshut solution was applied as background electrolyte in case of Ca-bentonite experiments. From the recorded emission spectra presented in Fig. 6, a different U(VI) speciation in the mineral suspensions at the two different solution conditions is apparent. A direct comparison of the recorded emission spectra of the alumosilicate samples in the two different pH-regimes can be found in Fig. S5.

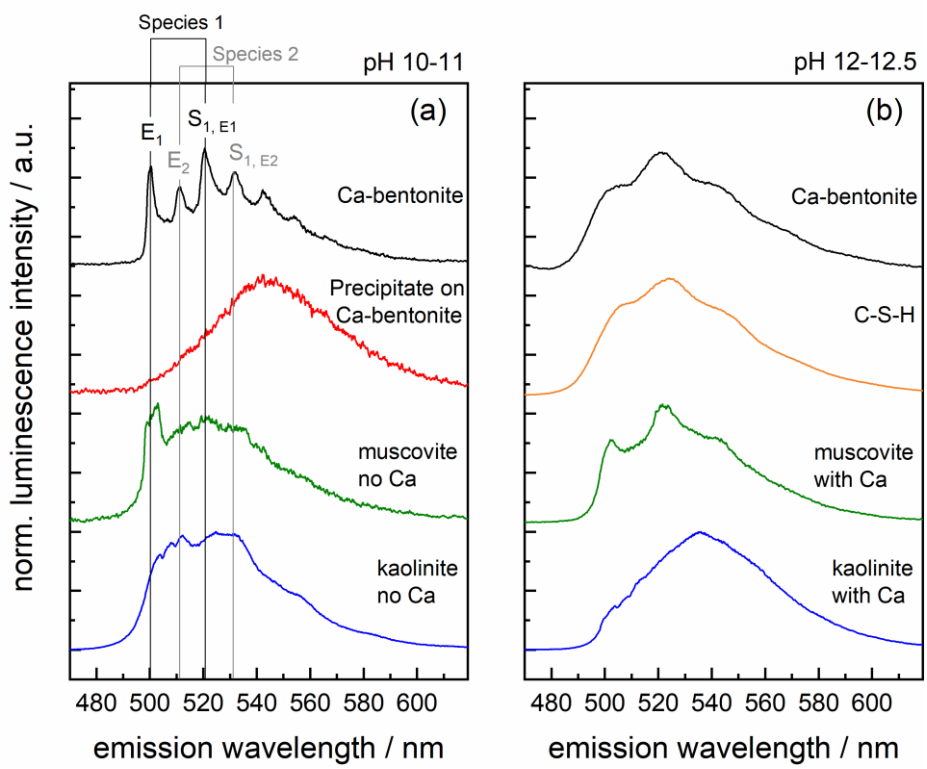

Figure 6: U(VI) emission spectra obtained from wet paste alumosilicate samples at pH 10–11 (a) and at pH 12–12.5 (b). The excitation wavelength used to obtain the emission spectrum and the pH value of the sample suspension were (a) kaolinite (λ_{ex} = 499.7 nm, pH 10), muscovite (λ_{ex} = 499.7 nm, pH 11), Ca-bentonite, sorbate and precipitate (λ_{ex} = 499.7 nm, pH 11) and (b) kaolinite (λ_{ex} = 499.7 nm, pH 12), muscovite (λ_{ex} = 499.7 nm, pH 12), Ca-bentonite (λ_{ex} = 496.7 nm, pH 12.5), C-S-H (λ_{ex} = 342.0 nm, pH 12.1; Ca/Si = 1.2). The U(VI) loading of Ca-bentonite, muscovite and kaolinite was 1.67×10^{-3} mol/kg, that of the C-S-H phase was 8.3×10^{-4} mol/kg and that of the 'precipitate on Ca-bentonite' was 1.7×10^{-1} mol/kg.

As described previously (Philipp et al., 2019), the emission spectrum of the Ca-bentonite sample at pH 11 (top, black spectrum) shows pronounced luminescence line-narrowing as a result of resonant excitation of single U(VI) species in the sample, using an excitation wavelength of 499.7 nm. For this sample as well as for the other alumosilicate ones, a low total U(VI) concentration of 5×10^{-7} M was used, corresponding to a U(VI) loading of 1.67×10^{-3} mol/kg, to suppress U(VI) (surface) precipitation.

For the sample 'precipitate on Ca-bentonite' with 5×10^{-5} M U(VI) (loading 1.7×10^{-1} mol/kg), however, a broad spectrum (red trace) is obtained, indicative of surface precipitation as a result of the much higher U(VI) concentration.

From the emission spectrum of Ca-bentonite with 5×10^{-7} M U(VI) at pH 11, two U(VI) species could be identified (Philipp et al., 2019). Species 1 is characterized by a resonant electronic transition line (E_1), followed by the lines of vibronic progression on E_1 ($S_{N,E1}$, only $S_{1,E1}$ is indicated in the figure) caused by the vibronic degeneracy of the electronic ground state. The same is true for species 2, however, here a non-resonant excitation takes place. The electronic transition line and the first vibronic progression line are indicated in the figure with E_2 and $S_{1,E2}$, respectively. The calculated stretch vibration frequencies (ν_s), obtained from the spacing between the first two peaks of each species (i.e., between E_1 and $S_{1,E1}$ and between E_2 and $S_{1,E2}$, respectively) are 781 ± 5 cm^{-1} for species 1 and 758 ± 12 cm^{-1} for species 2. Based on the lower stretch vibration frequency of species 2, implying a stronger coordination in the equatorial plane by coordinating ligands, this species has been assigned to an inner-sphere sorbed U(VI) complex. Species 1, on the other hand, was assigned to a U(VI) complex with outer-sphere character, based on additional X-ray absorption spectroscopic investigations. More specifically, the EXAFS data showed the presence of a surface complex with a structure resembling that of the $UO_2(OH)_4^{2-}$ aqueous species and no backscattering signal from surface Al/Si atoms. In the light of the results obtained in our batch sorption experiments, and the adsorption of Ca^{2+} on the bentonite surface, it is very likely that the sorption of the uranyl species is mediated by Ca^{2+}. Thus, the term Ca-mediated complex (species 1) will be used in the following text to describe this U(VI) species.

In comparison to the Ca-bentonite sample, the line-narrowing of muscovite and kaolinite at pH 10–11 (absence of added Ca^{2+}), is much less pronounced at the same excitation wavelength of 499.7 nm, Fig. 6a. Such inhomogeneous line broadening following selective excitation has previously been observed for U(VI) sorbed on TiO_2 by Tits et al. (2015). In the same study, the authors investigated U(VI) association with C-S-H phases, for which clear line-narrowing could be observed. As both the set-up for the spectroscopic studies as well as the aqueous chemistry and the total UO_2^{2+} concentration in the samples were identical for both TiO_2 and C-S-H, no apparent reason for the less

pronounced luminescence line-narrowing for U(VI) sorption on TiO_2 could be given. Combining the results obtained in the present study and those by Tits et al. (2015), only the spectra of U(VI) sorption experiments with Ca-bentonite and C-S-H phases show pronounced line-narrowing, while the spectra of U(VI) sorption samples with TiO_2, muscovite, and kaolinite do not. Common for Ca-bentonite and C-S-H phases is a swellable structure with an interlayer space that can accommodate water molecules and various counter ions for charge compensation. U(VI) has been shown to sorb in this interlayer space (Kowal-Fouchard et al., 2004; Kremleva et al., 2020; Olivelli et al., 2013). The other minerals, for which the pronounced line-narrowing could not be observed, do not feature such an accessible interlayer space. In muscovite, the interlayer is occupied by potassium cations, while in kaolinite the octahedral and tetrahedral sheets are held together with hydrogen bonds, without any interlayer cations. Thus, in muscovite and kaolinite U(VI) sorption is restricted to the edge sites, significantly reducing the reactive surface area in comparison to Ca-bentonite and C-S-H phases. The reduced reactive surface area causes the distance between the adjacent uranium species to approach the critical Förster distance (Hink et al., 2003), leading to homo-resonance energy transfer. Knowing the U(VI) loading of 1.67×10^{-3} mol/kg and the specific surface area of the minerals, it can be calculated that approx. 1.3, 10.1 and 4.5 uranium atoms are adsorbed on a 10 nm^2 surface area of Ca-bentonite, muscovite and kaolinite, respectively. Assuming that the sorbed atoms are homogeneously distributed at the surface, the distance between the single adsorbed U(VI) complexes is approx. 2.76 nm on Ca-bentonite, 0.99 nm on muscovite and 1.49 nm on kaolinite. Hence, the distance between the U atoms on muscovite and kaolinite is much closer to the critical Förster distance of 0.7 nm, calculated by Tits et al. (2015), compared to Ca-bentonite, where line-narrowing could be observed.

At pH 12 and in the presence of added Ca^{2+}, all recorded emission spectra, independent of the excitation wavelength, are broader than at pH 10–11, and for kaolinite a clear red-shift to higher wavelengths has occurred (Fig. 6b). This shift could be due to precipitation from oversaturated solutions, similarly to what was observed for the higher U(VI) concentration in contact with Ca-bentonite (sample ‘precipitate on Ca-bentonite’). For a direct comparison of these emission spectra, the reader is referred to Fig. S6. The spectra are discussed in more detail below, but this result corroborates the role of the interlayer space for additional uranium uptake, which is not available in

the case of kaolinite, thus leading to surface saturation and precipitation of non-sorbed uranium from solution.

To get a better insight into the U(VI) speciation of the alumosilicate phases, a decomposition of the measured U(VI) emission spectra of the Ca-bentonite suspension at pH 11 and of the C-S-H phase with a Ca/Si ratio of 1.2 (pH 12.1) was performed to extract spectra of single species. The well-resolved emission spectrum of U(VI) sorption on Ca-bentonite at pH 11 in diluted Gipshut solution can be described with two single components, denoted species 1 and species 2 (Fig. 7a). From the U(VI)-doped C-S-H phase, two species (species 3 and species 4) with clearly broader emission bands were obtained, Fig. 7b.

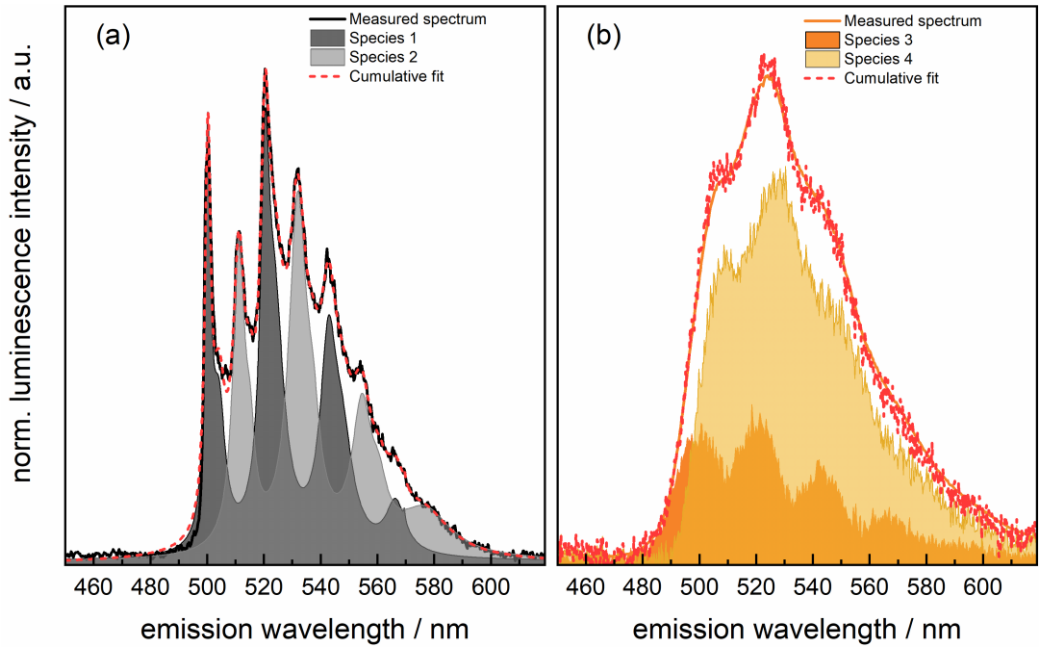

Figure 7: Extracted pure components from the decomposition of the measured U(VI) emission spectra in the Ca-bentonite suspension at pH 11 (a) and the C-S-H phase (Ca/Si = 1.2) at pH 12.1 (b).

Interestingly, the emission peak positions of species 1 and species 3 in the Ca-bentonite and the C-H-S sample, respectively, are very similar, pointing towards a similar U(VI) species in these systems (Fig. S7). The calculated stretch vibration frequency of this C-S-H species is 799 cm^{-1}, i.e., slightly higher than the ν_s for species 1 on Ca-bentonite (781 cm^{-1}). The second species in the C-S-H sample is slightly more red-shifted and has a stretch vibration frequency of 771 cm^{-1}.

In previous studies investigating U(VI) uptake by C-S-H phases with varying Ca/Si ratios, three types of U(VI) species were identified: (i) a surface complex, (ii) a species absorbed in the interlayer

region of C-S-H, sometimes referred to in the literature as an incorporated species and (iii) a precipitate, which is observed at increased U(VI) concentration (Tits et al., 2011; Tits et al., 2015; Wolter et al., 2019b). In C-S-H with Ca/Si 0.75-1.65 (Tits et al., 2011), the adsorbed species was characterized by an electronic transition line at 20,150 ± 60 cm^{-1} (496 nm) and ν_s ranging between 741 and 799 cm^{-1}. The interlayer sorbed species was clearly more red-shifted with E_1 = 19,824 ± 52 cm^{-1} (504 nm) and ν_s = 742–769 cm^{-1}. Its proportion was found to increase with time. By Tits et al. (2015), a C-S-H phase with a Ca/Si ratio of 1.07 was investigated with site-selective luminescence spectroscopy. As already mentioned, the samples showed pronounced line-narrowing allowing for a very precise determination of the stretch vibration frequencies of the two identified U(VI) species associated with the solid phase. The first species, which was assigned to an inner-sphere sorbed U(VI) species on the C-S-H surface yielded a ν_s of 758 ± 10 cm^{-1}. The second species, incorporated in the C-S-H structure, had a lower stretch vibration frequency of 744 ± 10 cm^{-1}. Thus, both species from Tits et al. (2015) have ν_s values which are lower than those of the species identified in the present study. However, the stretch vibration frequencies were found to increase with increasing excitation energy (ν_{ex}) (see Fig. 5 in Tits et al. (2015)), i.e., with decreasing excitation wavelengths (λ_{ex}). Thus, the differences in stretch vibration frequencies could be explained by the different excitation wavelengths applied in the respective studies: 476–530 nm for C-S-H (Tits et al., 2015), 499.7 nm for Ca-bentonite and 342 nm for C-S-H in the present investigation. Alternatively, a slightly different aqueous U(VI) speciation, arising from the different Ca/Si ratios and subsequently different equilibrium pH values in the study by Tits et al. (2015) and the current one, results in a slightly different U(VI) speciation on/in the C-S-H phase. At pH 12.1 (the equilibrium pH value of the C-S-H suspension in this study), the U(VI) speciation is dominated by the $UO_2(OH)_4^{2-}$ hydrolysis complex, while the $UO_2(OH)_3^-$ species is prevailing at slightly lower pH (10 < pH < 12).

Since species 3 in the C-S-H sample has a comparatively high stretch vibration frequency, indicating weaker binding in the equatorial plane by the surrounding ligands, and since the emission peak positions agree very well with those of species 1 found in our Ca-bentonite sample, we tentatively assign species 3 in the C-S-H sample to a Ca-mediated sorption complex on the C-S-H

surface. Species 4 in the C-S-H sample, on the other hand, is assumed to be absorbed in the C-S-H interlayer space, in agreement with previous studies.

To describe the measured spectra of the alumosilicate minerals obtained in the presence of 0.02 M Ca^{2+} at pH ≥ 12, the pure component spectra extracted from the Ca-bentonite and C-S-H samples (Fig. 7) as well as the spectrum of the surface precipitate on Ca-bentonite (as a pure component, without further spectral analysis) were used. Figure 8 shows that the composite emission spectra of the three different alumosilicates can be reproduced with the help of all four extracted emission spectra (species 1 and 2 on Ca-bentonite and species 3 and 4 on C-S-H) as well as the spectrum of the surface precipitate on Ca-bentonite.

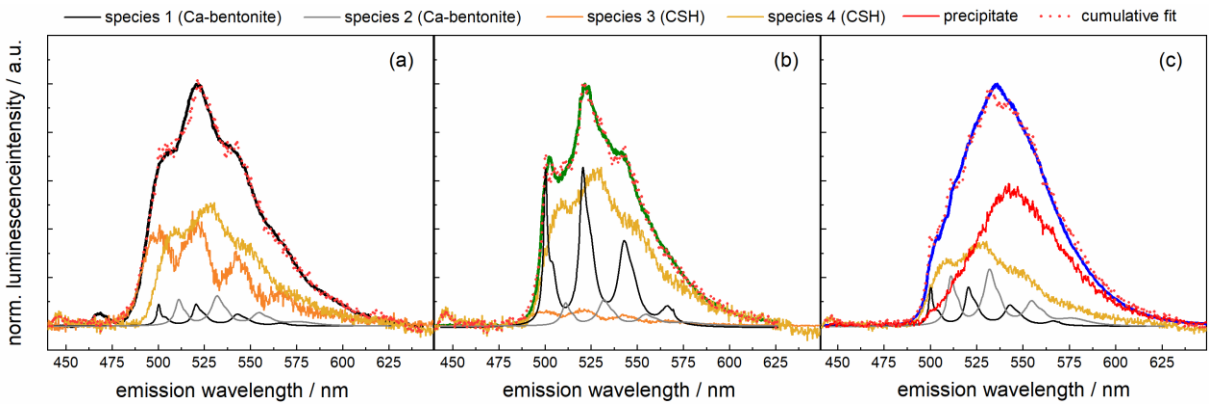

Figure 8: Results of spectral decomposition of the measured U(VI) emission spectra of Ca-bentonite, pH 12.5 (a), muscovite, pH 12 (b) and kaolinite, pH 12 (c) in the presence of 0.02 M $CaCl_2$.

In all cases, a very minor amount of the inner-sphere sorbed surface complex (species 2, Ca-bentonite) is present. In the kaolinite sample, the majority of the U(VI) signal stems from a surface precipitate, as already assumed based on the pronounced red-shift of this spectrum. In the muscovite and Ca-bentonite samples at pH 12, the Ca-mediated surface complex (species 1, Ca-bentonite) and both sorption complexes in the C-S-H sample (species 3 and 4) are required to explain the data. In both mineral suspensions, the major species is C-S-H species 4, closely followed by the Ca-mediated Ca-bentonite and C-S-H complexes (species 1 and 3, respectively). Note, exact percentages of the present species cannot be given due to the different excitation wavelengths used in the present study and the different luminescence quantum yields of the species. These results, however, clearly indicate that C-S-H phases are formed in all mineral suspensions when Ca is present in the system, and consequently, the U(VI) speciation is a mixture of Ca-mediated surface complexes on either the

556 alumosilicate mineral and/or the newly formed C-S-H phase (species 1 or 3), and species absorbed in
557 the C-S-H interlayer space (species 4). A detailed discussion of the underlying retention mechanisms,
558 combining the results of the batch sorption experiments and luminescence spectroscopy, follows in
559 section 3.4.

560 **3.4. Discussion of underlying retention mechanisms**

561 The batch sorption experiments with Ca-bentonite, synthetic and natural kaolinite, and muscovite
562 in different background electrolytes demonstrate that certain amounts of dissolved Ca^{2+} enable U(VI)
563 and Np(VI) retention at pH 10–13 despite the anionic character of prevailing aqueous species.

564 The TRLFS results reveal that the underlying U(VI) retention mechanisms are (i) sorption onto
565 the alumosilicate minerals, apparently facilitated by a bridging effect of Ca between the anionic
566 actinide complexes and the negatively charged mineral surfaces (Ca-mediated sorption), and (ii) inner-
567 sphere sorption in the interlayer region of C-S-H phases, which most likely form as secondary mineral
568 phases in the presence of Ca^{2+}. The inner-sphere sorption of U(VI) onto the primary alumosilicate
569 minerals plays only a minor role at hyperalkaline conditions. The retention mechanisms are discussed
570 below.

571 The proposed mechanism of Ca-bridging uranyl sorption is similar to so called type B ternary
572 surface complexation (Bradl, 2005; Hubbard, 2002). Such ternary type B surface complexes form by
573 coordination of a metal to a sorbed ligand, thus have the configuration surface ≡ ligand − metal. In
574 contrast to type B surface complexes, in the present study the metal (U(VI) or Np(VI)) is not only
575 bridged via the ligand (OH) but also via an additional metal cation (Ca^{2+} or Sr^{2+}) (surface ≡ Ca^{2+}/Sr^{2+} –
576 ligand – metal). Such complex systems, exceeding simple coordination of a metal to the surface or
577 ternary surface complexation, have not been studied thoroughly so far. Moreover, conventionally the
578 adsorption of ions to surfaces of opposite charge is studied. Sorption of anionic actinide complexes to
579 a negatively charged surface, as observed in the present work, is a rarely considered scenario. For
580 example, Yamaguchi et al. (2004) ruled out the sorption of anionic actinide complexes on negatively
581 charged mineral surfaces (pH 11–13.6), but suggested that only neutral actinide species sorbed.

A few studies already described the potential of Ca^{2+} to enhance anion retention in general. Allen et al. (2019) and Griffin et al. (2016) described a Ca-bridging between the anionic surfactant bis(2-ethylhexyl) sulfosuccinate and mica surfaces. The bridging effect was only observed in the presence of divalent cations and was absent in monovalent electrolyte solutions. Also Arnarson and Keil (2000) pointed out an increased sorption of natural organic matter to montmorillonite due to Ca-bridging. Furthermore, sorption experiments by Androniuk et al. (2017) revealed a mediating effect of Ca^{2+} between gluconate and C-S-H mineral surfaces, as the retention of the organic molecules strongly depended on the surface charge and Ca^{2+} concentration. For Np(V) and Np(VI), Tits et al. (2014) obtained higher retention on TiO_2 in the presence of Ca^{2+} at pH 13.3. The K_d value of Np(VI) increased by two orders of magnitude upon introduction of 10^{-5} M Ca^{2+}. The authors stated that additional experiments, especially spectroscopy, were necessary to draw conclusions regarding the underlying retention mechanisms.

The effect of Ca^{2+} on U(VI) adsorption was widely studied in the near-neutral to slightly alkaline pH range: Ca can either sorb to minerals, thus competing with RNs for surface sites, or the presence of Ca^{2+} might affect the aqueous RN speciation by forming stable ternary aqueous complexes (e.g., $Ca_2UO_2(CO_3)_{3(aq)}$, $CaUO_2(CO_3)_3^{2-}$) which show a decreased retention on minerals (Dong et al., 2005; Joseph et al., 2013a; Meleshyn et al., 2009; Philipp et al., 2019; Richter et al., 2016; Stockmann et al., 2022). In contrast, there are only few published and peer reviewed data in the alkaline to hyperalkaline pH range. In the batch sorption data of two Ph.D. theses, a Ca-induced increase in U(VI) sorption at (hyper)alkaline conditions was observed: Schnurr (2015) noticed a difference between U(VI) sorption on Illite du Puy in NaCl and $CaCl_2$ at pH 10–12. Mayordomo (2017) needed to introduce a Ca-mediated surface complex $S^WO\text{-}Ca\text{-}UO_2(OH)_3$ to be able to model elevated U(VI) sorption on smectite at pH 9.5–10. Only recently, Brix et al. (2021) described an increased U(VI) retention on Ca-bentonite in the presence of Ca^{2+} at pH 12.5 and 13 and proposed a bridging effect of Ca. The results of Philipp et al. (2019) and of the present study also strongly suggest such Ca-mediated surface complexes, even over a wider alkaline pH range.

Molecular dynamics (MD) and potential of mean force (PMF) calculations, performed for potential interactions in the system U(VI) – gluconate – C-S-H by Androniuk and Kalinichev (2020),

revealed several aspects that are important for the discussion of the proposed complexes in the present paper: (i) the interaction between $UO_2(OH)_3^-$ and Ca^{2+} ions in solution is strong, showing two main energy minima at interionic distances of ~4.1 Å and ~3.6 Å that correspond to the formation of one and two OH^- bridges, respectively. The interaction of U(VI) with $Ca(OH)^+$ and Na^+ is considered weak. (ii) The binding of Ca^{2+} on deprotonated silanol groups of the C-S-H surface is strong, can occur via inner- and outer-sphere coordination, and a relatively high energy is required to replace the bound cation by another ion or molecule. $Ca(OH)^+$ binding is less favorable. (iii) Compared to Ca^{2+} sorption, the sorption of $CaUO_2(OH)_3^+$ is weaker. (iv) U(VI) can bind directly to unoccupied deprotonated silanol groups and by the formation of ternary surface complexes between $UO_2(OH)_3^-$ and Ca^{2+} cations sorbed to negatively charged silanol groups on the aqueous C-S-H interface.

From these MD simulation results, we derive structures for two ternary surface complexes showing the Ca-bridge between silanol surface sites of the minerals and uranyl hydroxide species ($UO_2(OH)_3^-$, $UO_2(OH)_4^{2-}$) that represent our hypothesized retention mechanism (Fig. 9). These structures are further supported by our EXAFS results (Philipp et al., 2019), which demonstrated 4-fold coordination in the equatorial plane of U(VI) for the species. Moreover, the EXAFS results did not allow fitting of the U-Si/Al scattering paths for these species, which is indicative of a larger distance of the U(VI) moiety to the mineral surface. Our current luminescence spectroscopic study provides the so far missing spectroscopic evidence for the existence of such ternary U(VI) surface complexes at hyperalkaline conditions for Ca-bentonite and C-S-H phases, and in the presence of Ca^{2+} also for the clay minerals kaolinite and muscovite (see section 3.3.).

In the presence of Sr^{2+} instead of Ca^{2+}, similar surface complexes with Sr-bridges are conceivable since the speciation of Ca^{2+} and Sr^{2+} as a function of pH is very similar, with onset of hydrolysis at about pH 11.5 and dominance of $CaOH^+$ and $SrOH^+$ species above pH 13.1 and pH 13.7, respectively. Also for Sr^{2+}, inner-sphere sorption onto illite has been detected above pH 11 (Fuller et al., 2016).

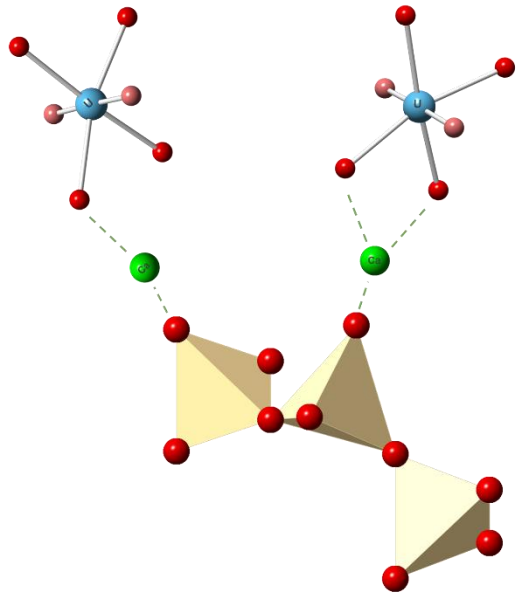

Figure 9: Proposed structure for ternary surface complexes showing exemplary the Ca-bridge between silanol surface sites of the minerals and uranyl hydroxide species predominant in the hyperalkaline pH range (see Fig. S4). Color code: uranium (blue), calcium (green), silicon (yellow), oxygen (red).

The second mechanism identified by TRLFS, for how the presence of Ca^{2+} enhances the U(VI) and Np(VI) immobilization at hyperalkaline conditions, is the formation of Ca-containing secondary minerals which are able to retain actinides. The contact of clay with hyperalkaline cement pore fluids results in partial dissolution of clay minerals and subsequent precipitation of secondary minerals such as calcium (aluminum) silicate hydrates (C-(A-)S-H), whereby also formation of zeolites, feldspathoids, feldspars and others was shown (Claret et al., 2002; Di Pietro et al., 2020; Fernandez et al., 2010; Gaucher and Blanc, 2006; Grambow, 2016; Sakamoto et al., 2007; Savage et al., 2007; Wilson et al., 2021). Enhanced dissolution of quartz, microcline, orthoclase, and albite has been observed in Ca-containing hyperalkaline solutions (Bagheri et al., 2022). C-(A-)S-H phases have been shown to form as secondary mineral phases in a so-called pozzolanic reaction in which available free Ca^{2+} reacts with dissolved mineral components (Bagheri et al., 2022; Cherian et al., 2018). Thus, a prerequisite for the formation of C-(A-)S-H phases is the partial dissolution of clay and silicate minerals above pH 10. In leaching tests, we observed significant release of Si and Al from the muscovite and the synthetic kaolinite at pH > 10. Leaching experiments with Ca-bentonite (Fig. S8) show a significant release of Si and Al into the solution only above pH 12, suggesting an apparent stability of the Ca-bentonite between pH 10 and 12. However, given the observed decrease in Ca

concentration in solution between pH 10 and 12, Si and Al could already be released from the clay minerals below pH 12, but immediately bound by precipitation of C-(A-)S-H phases. Leached Si and Al then only appear in the supernatant at pH > 12, when the availability of Ca becomes the limiting factor for C-(A-)S-H formation.

Due to the often amorphous or semi-crystalline character of C-(A-)S-H phases, their formation is difficult to detect with powder X-ray diffraction, especially when they precipitate as secondary minerals in multi-mineral solids such as bentonite. Weak diffraction signals from evolving C-(A-)S-H phases can easily be superimposed by the diffraction patterns of the primary minerals. Nevertheless, a small but distinct peak ($2\Theta = 29.3°$, Cu Kα) can be observed in the diffractograms of leached Ca-bentonite at pH 12 and 12.5, which is identified as a C-S-H phase by comparison with the diffractogram of the synthetically prepared C-S-H phase with a Ca/Si ratio of 1.2 (Fig. S9).

C-(A-)S-H phases show a high sorption capacity for trivalent to hexavalent actinides such as Cm(III), Am(III), Th(IV), Np(IV,V,VI), Pu(IV), and U(VI) (e.g., (Gaona et al., 2011; Häußler et al., 2018; Stumpf et al., 2004; Tits et al., 2014; Tits et al., 2015; Wolter et al., 2019a). C-S-H phase formation in Ca-montmorillonite at pH ≥ 12 with simultaneous incorporation of Cm(III) was previously hypothesized by Rabung et al. (2005). Our current luminescence spectroscopic study provides the spectroscopic evidence for the second retention mechanism in U(VI)-containing clay systems under hyperalkaline conditions, namely U(VI) absorption in the interlayer region of C-(A-)S-H phases, and thus also evidence for the formation of C-(A-)S-H phases in clay mineral systems under hyperalkaline conditions (see section 3.3.).

These results are in good agreement with the observed actinide retention on minerals in Ca-containing hyperalkaline solutions.

4. Conclusions

The results show that at (hyper)alkaline conditions, the presence of Ca^{2+} and Sr^{2+} has a major effect on the retention of hexavalent actinides on clay mineral surfaces. Alkaline earth ions can sorb on the mineral, thus, on the one hand, compete with the RNs for binding sites, but, on the other hand, mediate retention of anionic actinide species. While actinide sorption tends to be reduced due to

presence of Ca^{2+} in carbonate-containing solutions at neutral or slightly alkaline conditions, the actinide retention is enhanced by Ca at hyperalkaline conditions.

Our study verifies the hypothesis that negatively charged species $UO_2(OH)_3^-$, $UO_2(OH)_4^{2-}$ and $NpO_2(OH)_3^-$, $NpO_2(OH)_4^{2-}$, respectively, bind via Ca^{2+} cations to deprotonated surface groups of the alumosilicate minerals. Moreover, as a consequence of partial dissolution of the alumosilicates under hyperalkaline conditions, Ca^{2+} can induce a precipitation of secondary phases such as C-(A-)S-H, which additionally contribute to the retention of anionic actinide species in clayey systems, as demonstrated for the first time for U(VI) by luminescence spectroscopy. A combination of these processes leads to an increased U(VI) and Np(VI) retention at hyperalkaline conditions compared to chemical systems with exclusively monovalent cations in the background electrolytes.

In deep geological nuclear waste repositories, Ca^{2+} and other alkaline earth cations are ubiquitously present either in the pore water or as leachable ions in the host rock as well as in cement and bentonite as components of the multi-barrier system and consequently, contribute to the long-term retention of U(VI) and Np(VI) under the geochemical conditions prevailing in the repository. This deeper mechanistic understanding of actinide retention processes at hyperalkaline and high ionic strengths conditions contributes to an improved safety assessment of high-level waste repositories in deep geological formations.

CRediT authorship contribution statement

T. Philipp: Investigation, Formal analysis, Validation, Writing – review & editing.

N. Huittinen: Investigation, Formal analysis, Methodology, Writing – review & editing.

S. Shams Aldin Azzam: Investigation, Formal analysis.

R. Stohr: Investigation, Formal analysis.

J. Stietz: Investigation, Formal analysis.

T. Reich: Funding acquisition, Supervision, Writing – review & editing.

K. Schmeide: Conceptualization, Methodology, Funding acquisition, Project administration, Supervision, Writing – review & editing.

Declaration of competing interest

The authors declare that they have no known competing financial interests or personal relationships that could have appeared to influence the work reported in this paper.

Acknowledgements

The authors thank Samer Amayri (JGU Mainz) and Sabrina Beutner (HZDR) for ICP-MS analyses.

Funding

This work was supported by the German Federal Ministry for Economic Affairs and Energy (BMWi) within the projects GRaZ (no. 02E11415A, 02E11415B) and GRaZ II (no. 02E11860B).

Appendix A. Supplementary data

Supplementary data to this article can be found online at

References

Allen, F.J., Truscott, C.L., Gutfreund, P., Welbourn, R.J.L. and Clarke, S.M. (2019) Potassium, calcium, and magnesium bridging of AOT to mica at constant ionic strength. Langmuir 35, 5753-5761.

Amayri, S., Jermolajev, A. and Reich, T. (2011) Neptunium(V) sorption on kaolinite. Radiochim. Acta 99, 349-357.

Androniuk, I. and Kalinichev, A.G. (2020) Molecular dynamics simulation of the interaction of uranium(VI) with the C-S-H phase of cement in the presence of gluconate. Appl. Geochem. 113, 104496.

Androniuk, I., Landesman, C., Henocq, P. and Kalinichev, A.G. (2017) Adsorption of gluconate and uranyl on C-S-H phases: Combination of wet chemistry experiments and molecular dynamics simulations for the binary systems. Phys. Chem. Earth 99, 194-203.

Arnarson, T.S. and Keil, R.G. (2000) Mechanisms of pore water organic matter adsorption to montmorillonite. Marine Chem. 71, 309-320.

Atesok, G., Somasundaran, P. and Morgan, L.J. (1988) Adsorption properties of Ca^{2+} on Na-kaolinite and its effect on flocculation using polyacrylamides. Colloid Surface 32, 127-138.

Bagheri, M., Lothenbach, B., Shakoorioskooie, M. and Scrivener, K. (2022) Effect of different ions on dissolution rates of silica and feldspars at high pH. Cement Concrete Res. 152, 106644.

Berner, U.R. (1992) Evolution of pore water chemistry during degradation of cement in a radioactive waste repository environment. Waste Manage. 12, 201-219.

741 Bradl, H. (2005) Heavy Metals in the Environment: Origin, Interaction and Remediation, 1st Edition ed. Elsevier
742 Academic Press, London, UK.

743 Brix, K., Baur, S., Haben, A. and Kautenburger, R. (2021) Building the bridge between U(VI) and Ca-bentonite –
744 Influence of concentration, ionic strength, pH, clay composition and competing ions. Chemosphere 285,
745 131445.

746 Chen, X., Peng, S. and Wang, J. (2014) Retention profile and kinetics characteristics of the radionuclide 90-Sr(II)
747 onto kaolinite. J. Radioanal. Nucl. Chem. 303, 509-519.

748 Cherian, C., Kollannur, N.J., Bandipally, S. and Arnepalli, D.N. (2018) Calcium adsorption on clays: Effects of
749 mineralogy, pore fluid chemistry and temperature. Appl. Clay Sci. 160, 282-289.

750 Claret, F., Bauer, A., Schäfer, T., Griffault, L. and Lanson, B. (2002) Experimental investigation of the interaction
751 of clays with high-pH solutions: A case study from the Callovo-Oxfordian formation, Meuse-Haute Marne
752 underground laboratory (France). Clay Clay Miner. 50, 633-646.

753 Di Pietro, S., Emerson, H.P., Katsenovich, Y., Qafoku, N.P. and Szecsod, J. (2020) Phyllosilicate mineral
754 dissolution upon alkaline treatment under aerobic and anaerobic conditions. Appl. Clay Sci. 189, 105520.

755 Dong, W.M., Ball, W.P., Liu, C.X., Wang, Z.M., Stone, A.T., Bai, J. and Zachara, J.M. (2005) Influence of calcite
756 and dissolved calcium on uranium(VI) sorption to a Hanford subsurface sediment. Environ. Sci. Technol. 39,
757 7949-7955.

758 Farooq, U., Tweheyo, M.T., Sjöblom, J. and Øye, G. (2011) Surface characterization of model, outcrop, and
759 reservoir samples in low salinity aqueous solutions. J. Disper. Sci. Technol. 32, 519-531.

760 Fellhauer, D., Gaona, X., Rothe, J., Altmaier, M. and Fanghänel, T. (2018) Neptunium(VI) solubility in alkaline
761 $CaCl_2$ solutions: evidence for the formation of calcium neptunates Ca_xNpO_{3+x}(s,hyd). Monatsh. Chem. 149, 237-
762 252.

763 Fenter, P., Park, C., Nagy, K.L. and Sturchio, N.C. (2007) Resonant anomalous X-ray reflectivity as a probe of ion
764 adsorption at solid–liquid interfaces. Thin Solid Films 515, 5654-5659.

765 Fernandez, R., Rodriguez, M., de la Villa, R.V. and Cuevas, J. (2010) Geochemical constraints on the stability of
766 zeolites and C-S-H in the high pH reaction of bentonite. Geochim. Cosmochim. Acta 74, 890-906.

767 Fialips, C.-I., Petit, S., Decarreau, A. and Beaufort, D. (2000) Influence of synthesis pH on kaolinite "crystallinity"
768 and surface properties. Clay Clay Miner. 48, 173-184.

769 Fuller, A.J., Shaw, S., Peacock, C.L., Trivedi, D. and Burke, I.T. (2016) EXAFS study of Sr sorption to illite,
770 goethite, chlorite, and mixed sediment under hyperalkaline conditions. Langmuir 32, 2937-2946.

771 Gaona, X., Dähn, R., Tits, J., Scheinost, A.C. and Wieland, E. (2011) Uptake of Np(IV) by C-S-H phases and
772 cement paste: An EXAFS study. Environ. Sci. Technol. 45, 8765-8771.

773 Gaucher, E.C. and Blanc, P. (2006) Cement/clay interactions - A review: Experiments, natural analogues, and
774 modeling. Waste Manage. 26, 776-788.

775 Gaucher, E.C., Blanc, P., Bardot, F., Braibant, G., Buschaert, S., Crouzet, C., Gautier, A., Girard, J.P., Jacquot, E.,
776 Lassin, A., Negrel, G., Tournassat, C., Vinsot, A. and Altmann, S. (2006) Modelling the porewater chemistry of
777 the Callovian-Oxfordian formation at a regional scale. C. R. Geosci. 338, 917-930.

778 Grambow, B. (2016) Geological disposal of radioactive waste in clay. Elements 12, 239-245.

779 Griffin, L.R., Browning, K.L., Lee, S.Y., Skoda, M.W., Rogers, S. and Clarke, S.M. (2016) Multilayering of calcium
780 aerosol-OT at the mica/water interface studied with neutron reflection: Formation of a condensed lamellar
781 phase at the CMC. Langmuir 32, 13054-13064.

Häußler, V., Amayri, S., Beck, A., Platte, T., Stern, T.A., Vitova, T. and Reich, T. (2018) Uptake of actinides by calcium silicate hydrate (C-S-H) phases. Appl. Geochem. 98, 426-434.

He, Y., Chen, Y.-G. and Ye, W.-M. (2016) Equilibrium, kinetic, and thermodynamic studies of adsorption of Sr(II) from aqueous solution onto GMZ bentonite. Environ. Earth Sci. 75, 807.

Hellebrandt, S. (2017) Grenzflächenreaktionen von Actiniden an Muskovit. Ph.D. thesis, Technische Universität Dresden, Dresden, Germany.

Hennig, T., Stockmann, M. and Kühn, M. (2020) Simulation of diffusive uranium transport and sorption processes in the Opalinus Clay. Appl. Geochem. 123, 104777.

Hink, M.A., Visser, N.V., Borst, J.W., van Hoek, A. and Visser, A.J.W.G. (2003) Practical use of corrected fluorescence excitation and emission spectra of fluorescent proteins in Förster Resonance Energy Transfer (FRET) studies. J. Fluoresc. 13, 185-188.

Ho, C. and Handy, R.L. (1963) Electrokinetic properties of lime-treated bentonites. Clay Clay Miner. 12, 267-280.

Hubbard, A.T. (2002) Encyclopedia of Surface and Colloid Science. Dekker, New York (USA); Basel (Switzerland).

Huittinen, N., Rabung, T., Andrieux, P., Lehto, J. and Geckeis, H. (2010) A comparative batch sorption and time-resolved laser fluorescence spectroscopy study on the sorption of Eu(III) and Cm(III) on synthetic and natural kaolinite. Radiochim. Acta 98, 613-620.

Jenni, A., Wersin, P., Thoenen, T., Baeyens, B., Ferrari, A., Gimmi, T., Mäder, U., Marschall, P., Hummel, W. and Leupin, O. (2019) Bentonite backfill performance in a high-level waste repository: a geochemical perspective. Nagra Technical Report 19-03, Nagra, Wettingen, Switzerland.

Joseph, C., Mibus, J., Trepte, P., Müller, C., Brendler, V., Park, D.M., Jiao, Y., Kersting, A.B. and Zavarin, M. (2017) Long-term diffusion of U(VI) in bentonite: Dependence on density. Sci. Total Environ. 575, 207-218.

Joseph, C., Stockmann, M., Schmeide, K., Sachs, S., Brendler, V. and Bernhard, G. (2013a) Sorption of U(VI) onto Opalinus Clay: Effects of pH and humic acid. Appl. Geochem. 36, 104-117.

Joseph, C., Van Loon, L.R., Jakob, A., Steudtner, R., Schmeide, K., Sachs, S. and Bernhard, G. (2013b) Diffusion of U(VI) in Opalinus Clay: Influence of temperature and humic acid. Geochim. Cosmochim. Acta 109, 74-89.

Kaufhold, S. and Dohrmann, R. (2016) Distinguishing between more and less suitable bentonites for storage of high-level radioactive waste. Clay Min. 51, 289-302.

Kowal-Fouchard, A., Drot, R., Simoni, E. and Ehrhardt, J. (2004) Use of spectroscopic techniques for uranium(VI)/montmorillonite interaction modeling. Environ. Sci. Technol. 38, 1399-1407.

Kremleva, A., Krüger, S. and Rösch, N. (2020) Uranyl(VI) sorption in calcium silicate hydrate phases. A quantum chemical study of tobermorite models. Appl. Geochem. 113, 104463.

Lommerzheim, M. and Jobmann, A. (2014) Endlagerkonzept sowie Verfüll- und Verschlusskonzept für das Standortmodell NORD, TEC-08-2014-Z. DBE Technology, Peine, Germany.

Marques Fernandes, M., Baeyens, B., Dähn, R., Scheinost, A.C. and Bradbury, M.H. (2012) U(VI) sorption on montmorillonite in the absence and presence of carbonate: A macroscopic and microscopic study. Geochim. Cosmochim. Acta 93, 262-277.

Marsac, R., Banik, N.L., Lützenkirchen, J., Diascorn, A., Bender, K., Marquardt, C.M. and Geckeis, H. (2017) Sorption and redox speciation of plutonium at the illite surface under highly saline conditions. J. Colloid Interface Sci. 485, 59-64.

Mayordomo, N. (2017) Experimental and theoretical studies of mixed smectite and Al_2O_3 nanoparticles to improve pollutant retention in geochemical barriers. Ph.D. thesis, Departamento de Química Analítica, Química Física e Ingeniería Química. Universidad de Alcalá, Madrid, Spain.

Meleshyn, A., Azeroual, M., Reeck, T., Houben, G., Riebe, B. and Bunnenberg, C. (2009) Influence of (calcium-)uranyl-carbonate complexation on U(VI) sorption on Ca- and Na-bentonites. Environ. Sci. Technol. 43, 4896–4901.

Missana, T. and García-Gutiérrez, M. (2007) Adsorption of bivalent ions (Ca(II), Sr(II) and Co(II)) onto FEBEX bentonite. Phys. Chem. Earth, Parts A/B/C 32, 559-567.

Missana, T., Garcia-Gutierrez, M. and Alonso, U. (2008) Sorption of strontium onto illite/smectite mixed clays. Phys. Chem. Earth, Parts A/B/C 33, S156-S162.

Nagasaki, S., Saito, T. and Yang, T.T. (2016) Sorption behavior of Np(V) on illite, shale and MX-80 in high ionic strength solutions. J. Radioanal. Nucl. Chem. 308, 143-153.

Nowak, T. and Maßmann, J. (2013) Endlagerstandortmodell Nord (AnSichT) - Teil III: Auswahl von Gesteins- und Fluideigenschaften für numerische Modellberechnungen im Rahmen des Langzeitsicherheitsnachweises. Bundesanstalt für Geowissenschaften und Rohstoffe (BGR), Hannover, Germany.

OECD/NEA (2020) Management and Disposal of High-Level Radioactive Waste: Global Progress and Solutions, Radioactive Waste Management, OECD Publishing, Paris, https://doi.org/10.1787/33f65af2-en.

Olivelli, M.S., Curutchet, G.A. and Sanchez, R.M.T. (2013) Uranium uptake by montmorillonite-biomass complexes. Ind. Eng. Chem. Res. 52, 2273-2279.

Philipp, T., Shams Aldin Azzam, S., Rossberg, A., Huittinen, N., Schmeide, K. and Stumpf, T. (2019) U(VI) sorption on Ca-bentonite at (hyper)alkaline conditions - Spectroscopic investigations of retention mechanisms. Sci. Total Environ. 676, 469-481.

Pointeau, I., Reiller, P., Mace, N., Landesman, C. and Coreau, N. (2006) Measurement and modeling of the surface potential evolution of hydrated cement pastes as a function of degradation. J. Colloid Interface Sci. 300, 33-44.

Pruett, R.J. and Webb, H.L. (1993) Sampling and analysis of KGa-1b well-crystallized kaolin source clay. Clay Clay Miner. 41, 514-519.

Rabung, T., Pierret, M.C., Bauer, A., Geckeis, H., Bradbury, M.H. and Baeyens, B. (2005) Sorption of Eu(III)/Cm(III) on Ca-montmorillonite and Na-illite. Part 1: Batch sorption and time-resolved laser fluorescence spectroscopy experiments. Geochim. Cosmochim. Acta 69, 5393-5402.

Richter, C., Müller, K., Drobot, B., Steudtner, R., Großmann, K., Stockmann, M. and Brendler, V. (2016) Macroscopic and spectroscopic characterization of uranium(VI) sorption onto orthoclase and muscovite and the influence of competing Ca^{2+}. Geochim. Cosmochim. Acta 189, 143-157.

Sakamoto, H., Shibata, M., Owada, H., Kaneko, M., Kuno, Y. and Asano, H. (2007) Development of an analytical technique for the detection of alteration minerals formed in bentonite by reaction with alkaline solutions. Phys. Chem. Earth 32, 311-319.

Savage, D., Walker, C., Arthur, R., Rochelle, C., Oda, C. and Takase, H. (2007) Alteration of bentonite by hyperalkaline fluids: A review of the role of secondary minerals. Phys. Chem. Earth 32, 287-297.

Schlegel, M.L., Nagy, K.L., Fenter, P., Cheng, L., Sturchio, N.C. and Jacobsen, S.D. (2006) Cation sorption on the muscovite (001) surface in chloride solutions using high-resolution X-ray reflectivity. Geochim. Cosmochim. Acta 70, 3549-3565.

Schmeide, K. and Bernhard, G. (2010) Sorption of Np(V) and Np(IV) onto kaolinite: Effects of pH, ionic strength, carbonate and humic acid. Appl. Geochem. 25, 1238-1247.

Schnurr, A. (2015) Untersuchungen zur Radionuklidsorption an Tonmineraloberflächen bei hohen Ionenstärken. Ph.D. thesis, Karlsruher Institut für Technologie (KIT), Karlsruhe, Germany.

Schnurr, A., Marsac, R., Rabung, T., Lützenkirchen, J. and Geckeis, H. (2015) Sorption of Cm(III) and Eu(III) onto clay minerals under saline conditions: Batch adsorption, laser-fluorescence spectroscopy and modeling. Geochim. Cosmochim. Acta 151, 192-202.

Scholze, R., Amayri, S. and Reich, T. (2019) Modeling the sorption of Np(V) on Na-montmorillonite - effects of pH ionic strength and CO_2. Radiochim. Acta 107, 615-622.

Stockmann, M., Fritsch, K., Bok, F., Marques Fernandes, M., Baeyens, B., Steudtner, R., Müller, K., Nebelung, C., Brendler, V., Stumpf, T. and Schmeide, K. (2022) New insights into U(VI) sorption onto montmorillonite from batch sorption and spectroscopic studies at increased ionic strength. Sci. Total Environ. 806, 150653.

Stumpf, T., Tits, J., Walther, C., Wieland, E. and Fanghänel, T. (2004) Uptake of trivalent actinides (curium(III)) by hardened cement paste: a time-resolved laser fluorescence spectroscopy study. J. Colloid Interf. Sci. 276, 118-124.

Sugiura, Y., Ishidera, T. and Tachi, Y. (2021) Surface complexation of Ca and competitive sorption of divalent cations on montmorillonite under alkaline conditions. Appl. Clay Sci. 200, 105910.

Szymanek, K., Charmas, R. and Piasecki, W. (2021) Investigations of mechanism of Ca^{2+} adsorption on silica and alumina based on Ca-ISE monitoring, potentiometric titration, electrokinetic measurements and surface complexation modeling. Adsorption 27, 105-115.

Tits, J., Gaona, X., Laube, A. and Wieland, E. (2014) Influence of the redox state on the neptunium sorption under alkaline conditions: Batch sorption studies on titanium dioxide and calcium silicate hydrates. Radiochim. Acta 102, 385-400.

Tits, J., Geipel, G., Macé, N., Eilzer, M. and Wieland, E. (2011) Determination of uranium(VI) sorbed species in calcium silicate hydrate phases: A laser-induced luminescence spectroscopy and batch sorption study. J. Colloid Interface Sci. 359, 248-256.

Tits, J., Walther, C., Stumpf, T., Mace, N. and Wieland, E. (2015) A luminescence line-narrowing spectroscopic study of the uranium(VI) interaction with cementitious materials and titanium dioxide. Dalton Trans. 44, 966-976.

Tran, E.L., Teutsch, N., Klein-BenDavid, O. and Weisbrod, N. (2018) Uranium and cesium sorption to bentonite colloids under carbonate-rich environments: Implications for radionuclide transport. Sci. Total Environ. 643, 260-269.

Viallis-Terrisse, H., Nonat, A. and Petit, J.-C. (2001) Zeta-potential study of calcium silicate hydrates interacting with alkaline cations. J. Colloid Interface Sci. 244, 58-65.

Wieland, E., Wanner, H., Albinsson, Y., Wersin, P. and Karnland, O. (1994) A surface chemical model of the bentonite-water interface and its implications for modelling the near field chemistry in a repository for spent fuel. Swedish Nuclear Fuel and Waste Management Company (SKB), Stockholm, Sweden.

Wilson, J., Bateman, K. and Tachi, Y. (2021) The impact of cement on argillaceous rocks in radioactive waste disposal systems: A review focusing on key processes and remaining issues. Appl. Geochem. 130, 104979.

Wolfgramm, M., Thorwart, K., Rauppach, K. and Brandes, J. (2011) Zusammensetzung, Herkunft und Genese geothermaler Tiefengrundwässer im Norddeutschen Becken (NDB) und deren Relevanz für die geothermische Nutzung. Z. Geol. Wissenschaft 339, 173-193.

Wolter, J.-M., Schmeide, K., Huittinen, N. and Stumpf, T. (2019a) Cm(III) retention by calcium silicate hydrate (C-S-H) gel and secondary alteration phases in carbonate solutions with high ionic strength: A site-selective TRLFS study. Sci. Rep. 9, 14255.

Wolter, J.-M., Schmeide, K., Weiss, S., Bok, F., Brendler, V. and Stumpf, T. (2019b) Stability of U(VI) doped calcium silicate hydrate gel in repository-relevant brines studied by leaching experiments and spectroscopy. Chemosphere 218, 241-251.

Wu, T., Amayri, S., Drebert, J., Van Loon, L.R. and Reich, T. (2009) Neptunium(V) sorption and diffusion in Opalinus Clay. Environ. Sci. Technol. 43, 6567-6571.

Yamaguchi, T., Nakayama, S. and Yoshida, T. (2004) Interactions between anionic complex species of actinides and negatively charged mineral surfaces. Radiochim. Acta 92, 677-682.